An experimentally-based molecular dynamics analysis of grain boundary migration during recrystallization in aluminum

Li, Runguang; Homer, Eric R.; Hong, Chuanshi; Zhang, Yubin; Jensen, Dorte Juul

Published in:
Scripta Materialia

Link to article, DOI:
10.1016/j.scriptamat.2021.114489

Publication date:
2022

Document Version
Publisher's PDF, also known as Version of record

Scripta Materialia 211 (2022) 114489

Contents lists available at ScienceDirect

Scripta Materialia

journal homepage: www.elsevier.com/locate/scriptamat

An experimentally-based molecular dynamics analysis of grain boundary migration during recrystallization in aluminum

Runguang Li[a,*], Eric R. Homer[b], Chuanshi Hong[c], Yubin Zhang[a], Dorte Juul Jensen[a]

[a] Department of Mechanical Engineering, Technical University of Denmark, Kongens Lyngby DK-2800, Denmark
[b] Department of Mechanical Engineering, Brigham Young University, Provo, UT 84602, USA
[c] Shenyang National Laboratory for Materials Science, Institute of Metal Research, Chinese Academy of Sciences, Shenyang 110016, China

ARTICLE INFO

Article history:
Received 5 November 2021
Revised 20 December 2021
Accepted 26 December 2021
Available online 4 January 2022

Keywords:
Recrystallization
Grain boundary mobility
Molecular dynamics

ABSTRACT

Recent synchrotron X-ray measurements examined three-dimensional boundary migration during recrystallization [Scripta Mater 205 (2021) 114187]. To analyze possible correlations between grain boundary mobility and the observed heterogeneous boundary migration, molecular dynamics simulations were carried out. Migration of two selected boundary segments were simulated in both planar and spherical bicrystal atomistic models. These two segments were chosen because in the experiment one was observed to migrate much faster than the other. The simulations reveal that mobility cannot account for the experimentally observed heterogeneous migration. The result points to the possibility that recrystallization boundary migration strongly depends on features within the deformed microstructure.

Recrystallization is one of the most effective approaches to alter microstructures. The main driving force for recrystallization is the energy stored in the deformed matrix [1]. When a deformed metal is heat-treated, new nearly defect-free grains emerge and grow to replace the deformed matrix, leading to a significant change in grain size, morphology, and texture compared to the deformed and original states, thus changing the mechanical and physical properties. Understanding the local mechanisms governing the boundary migration during recrystallization and factors influencing the migration is of utmost scientific interest and essential for industrial processing.

Grain boundary (GB) migration has been examined by experimental observations for more than one century [2]. During the past decades, new results contradicting common wisdom have however been reported [3–6]. Based on the development of three-dimensional (3D) X-ray microscopy techniques, the growth of grains during recrystallization in bulk polycrystalline metals has been characterized both by *in-situ* and *ex-situ* studies [7–10]. The crystallographic orientations in these investigations were recorded for each 3D voxel with a spatial resolution in the micron to submicron scale. The full voxelized maps of microstructures revealed heterogeneous growth patterns, with irregular retrusions and protrusions of different amplitudes and widths. Zhang et al. [7] demonstrated that curvature driving and dragging forces related to sharp retrusions and protrusions can play a significant role on migrating recrystallization boundaries in addition to the stored energy driving force. It has also been suggested that the size and shape of the retrusions and protrusions are correlated in a relatively complex way to the spatial variations of the stored energy in the deformed microstruture [7], and that the deformation microstructure morphology is of key importance for recrystallization [11].

While GB mobility is a property known to control how fast a boundary will migrate during grain growth (depending upon the magnitude of driving force applied) [12,13], it is unclear how the GB mobility will affect recrystallization under the heterogeneous conditions provided by the deformation microstructure. Furthermore, understanding the intrinsic GB mobility is still complicated as the mobility depends on temperature and GB crystallography. The latter has five degrees of freedom on the mesoscale (and even more on the atomic scale), and as a result, the variability of GB mobility with GB crystallography is not well understood.

The purpose of this paper is to use atomistic simulations to understand the role that the intrinsic GB mobility for different boundary plane (BP) normals may play in boundary migration during recrystallization. The system we have chosen is one examined in a recent 3D experiment [14] which reveals similar stored energy for a migrating and non-migrating boundary segment, but with different BP normal and dislocation structures in front of the two segments. In an experiment, the influence of energy and mobility cannot be separated. However, the combination of experiment and simulation, where experimental results are used as input to

* Corresponding author.
E-mail address: rulia@dtu.dk (R. Li).

https://doi.org/10.1016/j.scriptamat.2021.114489

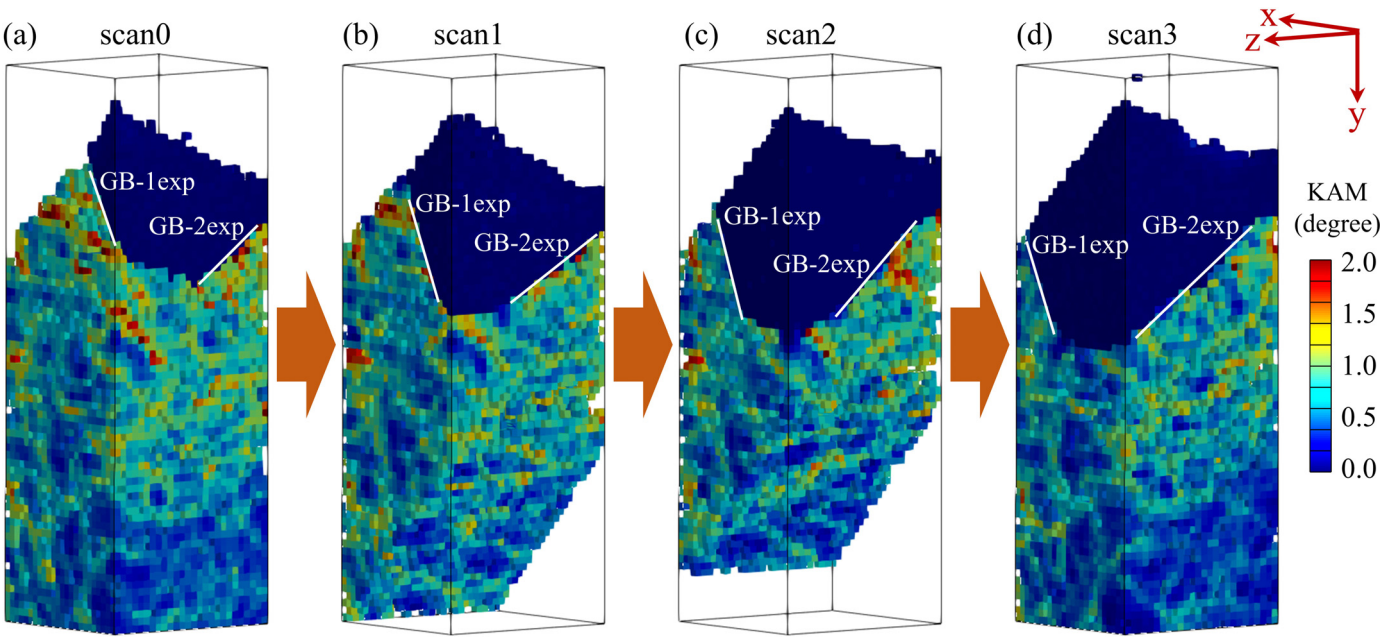

Fig. 1. Snapshots of the growth of the selected grain during recrystallization of a 12% cold-rolled aluminum single crystal [14]. The nucleation of the grain was stimulated by a hardness indent. (a) Scan0. (b) Scan1. (c) Scan2. (d) Scan3. Voxels are colored by the kernel average misorientation (KAM).

the simulations, allows one to interpret unambiguously the experimentally observed migration.

As reported in detail in [14], a well-annealed high purity aluminum plate was rolled at room temperature to a thickness reduction of 12%, and a Vickers hardness indent was made on one surface followed by an annealing treatment (335 °C for 10 min) to obtain an initial recrystallizing grain. The growth of this grain was followed during recrystallization by white-beam differential-aperture X-ray microscopy (DAXM) in 4 scans. Fig. 1 plots snapshots of the grain from scan0 to scan3, clearly revealing the heterogeneous recrystallization boundary migration of different boundary segments, for which the BP normals differ significantly. Two boundary segments representing a migrating and a non-migrating boundary are identified as GB-1exp and GB-2exp, respectively, and marked in Fig. 1a–d. The voxelized data is used to calculate the boundary parameters, *i.e.*, misorientations and BP orientations. These boundaries (with misorientations of ∼20° and ∼15°) are high angle boundaries, and their relative mobility difference is unknown. While GB-2exp remains stationary, GB-1exp migrates and the BP normal changes from scan0 to scan1, see Fig. 2, and this change is considered in the simulations.

The resolved parameters serve as input data for atomistic simulations of boundary mobility where two types of molecular dynamics (MD) models are used: one with planar bicrystal grain boundaries, each with a single BP orientation, and one with spherical bicrystal grain boundaries that simultaneously examine all possible BP orientations.

First, as the experimentally measured misorientations in this study do not belong to any special GBs that have low-Σ coincidence site lattice (CSL) misorientations, we identify the nearest misorientation from among all possible CSLs with Σ values less than 1000. CSL misorientations are used in the simulations rather than the measured misorientations because the use of CSLs ensures periodicity in the GB plane, allowing us to avoid the effects of free surfaces, which can have a dramatic effect on MD simulations. GB-1exp and GB-2exp are most closely aligned with the Σ405b and Σ515b CSLs, respectively. The crystallographic parameters for the CSLs are given in Table 1. It is noted that the rotation axis of Σ405b and Σ515b deviate 2.28° and 1.52° from the experimental measurements, and 0.34° and 0.08° in rotation angle, respectively. While not exact, the selected CSLs are close to experimental observations and are deemed suitable for the present simulations.

Second, we identify relevant BP orientations for the conventional planar GBs in this work to match with those identified in the experiments. Two Σ405b GBs, named as GB-1sim-scan0 and GB-1sim-scan1, with BP orientations of $(\overline{169}\ 83\ 55)$ and $(\overline{661}\ 617\ 565)$ as well as one Σ515b GB, named GB-2sim-scan0, with a BP orientation of $(\bar{3}\ \overline{14}\ 1)$ are identified from the voxelized data. These BP orientations are all defined relative to the coordinates of the recrystallized grain though it is worth noting that these three BP orientations defined in the BP fundamental zones [15] are given as $(65\ 145\ 115)/(\overline{55}\ \overline{169}\ \overline{83})$, $(659\ 523\ 655)/(\overline{565}\ \overline{661}\ \overline{617})$, and $(1\ \bar{6}\ 13)/(1\ 3\ \overline{14})$, respectively. The BP orientations of the measured and simulated GBs are shown in a stereographic projection in Fig. 2, where the axes of the stereographic projection are aligned with the crystal axes of one of the crystals; The BP normal of GB-1sim-scan0, GB-1sim-scan1, and GB-2sim-scan0 deviates 0.59°, 0.69°, and 2.24° from the experimentally measured, respectively. It proved impossible to find BP orientation exactly consistent with the experiments that had reasonable simulation cell dimensions.

For the conventional planar bicrystal model, standard methods are used to construct a completely planar GB with a single BP in a monoclinic simulation cell [16,17]. A minimum energy structure is determined from sampling over variations of several GB construction parameters, *i.e.*, the relative placement of the two crystals at the GB, BP position, and the allowed proximity of GB atoms. Each structure from the set of possibilities is then minimized using the conjugate-gradient energy algorithm, after which the overall minimum energy structure is selected to represent the target GB. The aluminum embedded-atom method (EAM) interatomic potential developed by Mishin et al. [18] is utilized in LAMMPS [19] for atomistic simulations here. The minimum energy configurations are illustrated in supplementary Fig. S1. At last, mobilities are calculated by utilizing the Energy-Conserving Orientational (ECO) driving force method [20,21]. This method uses an additional artificial energy that varies depending on the crystal orientation, inducing an energy gradient across the GB, which leads to an artificial driving force to the atoms. The force drives GB migration

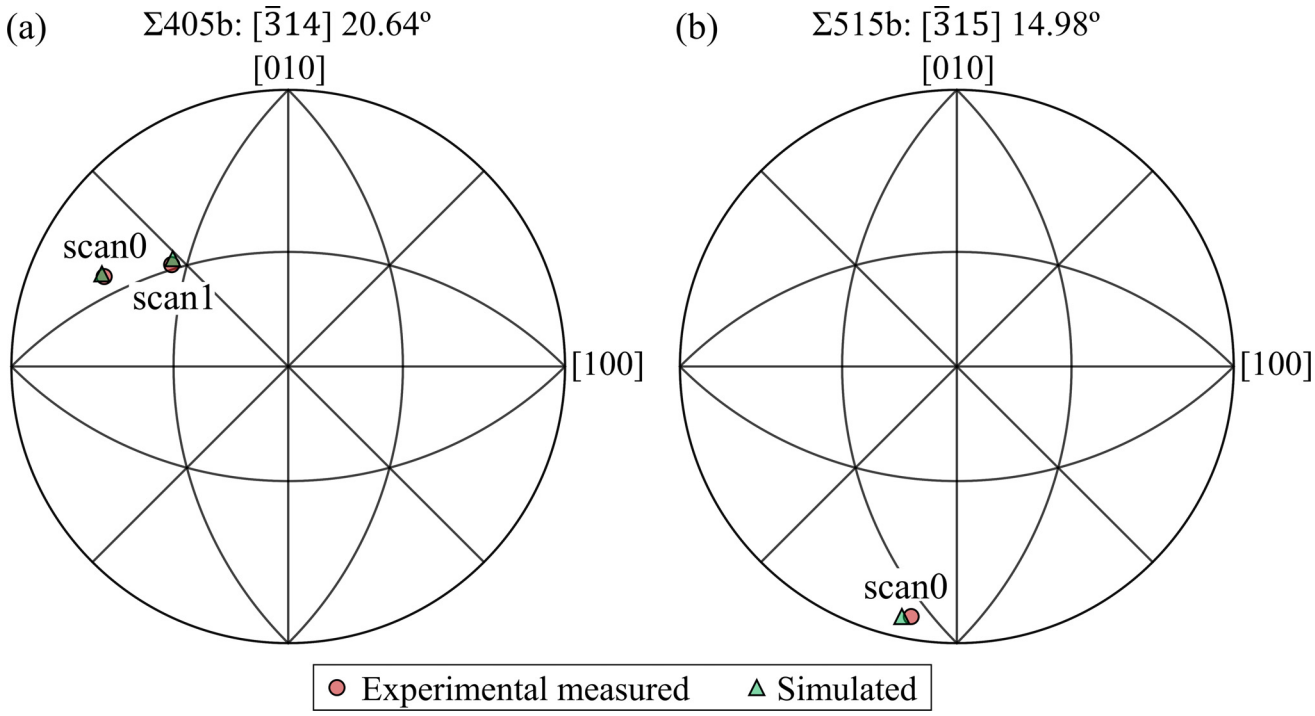

Fig. 2. Equal angle projection of boundary plane normal distributions for the experimentally measured and simulated GBs. (a) GB-1exp/sim-scan0/scan1. (b) GB-2exp/sim-scan0. The reference frame for the projection is the crystallographic coordinate system of the recrystallized grain.

Table 1
Parameters of the measured and selected grain boundaries.

GB	CSL	Rotation axis	Rotation angle	GB plane normal
GB-1exp-scan0		[−0.571 0.182 0.800]	20.3°	[−0.858 0.424 0.290]
GB-1sim-scan0	Σ405b	[$\bar{3}$ 1 4]	20.64°	[$\overline{169}$ 83 55]
GB-1exp-scan1		[−0.571 0.182 0.800]	20.3°	[-0.626 0.569 0.534]
GB-1sim-scan1	Σ405b	[$\bar{3}$ 1 4]	20.64°	[$\overline{661}$ 617 565]
GB-2exp-scan0		[−0.529 0.152 0.835]	14.9°	[−0.174 −0.981 0.086]
GB-2sim-scan0	Σ515b	[$\bar{3}$ 1 5]	14.98°	[$\bar{3}$ $\overline{14}$ 1]

Table 2
Calculated mobilities and activation energies for selected grain boundaries.

GB	Mobility (m s^{-1} GPa^{-1}) 400 K	600 K	800 K	Activation energy (eV)
GB-1sim-scan0	3.34	53.5	181	0.101
GB-1sim-scan1	2.11	21.7	80.8	0.039
GB-2sim-scan0	20.8	129	350	0.027

and growth of the grain with the favored orientation. Having the magnitude of the driving force (f) and the measured GB migration velocity (v), one can calculate the GB mobility (M) according to $v = M \times f$ [22].

As the experimental annealing temperature was 335 °C (608.15 K), the simulations were performed at 400 K, 600 K, and 800 K for a maximum annealing time of 400 ps. Fig. 3a–c plot the average positions as a function of annealing time for GB-1sim-scan0, GB-1sim-scan1, and GB-2sim-scan0, observing no abnormal migration behaviors for either of the boundaries. The mobilities of the three simulated GBs are calculated and plotted in an Arrhenius manner in Fig. 3d, showing a temperature-dependent trend in mobility. The calculated mobility and activation energy values are listed in Table 2. The result suggests that GB-2sim-scan0 has a higher migration ability than the two GB-1sim boundaries, which is contrary to experimental observations. The activation energy results do not provide an apparent contribution to the interpretation of observed GB migration behavior either, especially considering the fact that there is only a small difference between GB-2sim-scan0 and GB-1sim-scan1 but a large difference between the two GB-1sim boundaries. Neither the difference in crystallography nor GB character, and thus the difference in the intrinsic mobility, can explain why the different segments of the recrystallizing boundary in the experiments migrate or don't migrate.

One may speculate if the employed GB parameters in the simulations, especially the BP orientations, are too far from the experimental measurements. As there are no suitable misorientations or BP orientations in the planar bicrystal model that match better the experiments, and as we cannot estimate the uncertainty introduced by these approximations, we also used a spherical bicrystal simulation model to supplement the analysis.

For the spherical bicrystal model, a periodic block of the matrix grain is created with the crystal [100], [010], and [001] directions along the reference x, y, and z axes, respectively. The size of the block is set to be 400 Å along each coordinate direction containing a total of ~3.86 million atoms. Next, a spherical region with a radius of 190 Å at the center of the simulation domain is rotated until the two grains satisfy the experimentally measured misorientation listed in Table 1. The following procedures: the minimum energy structure searching, thermalization, and GB migration simulation, are conducted using the same methods as in the conventional bicrystal model, though it is noted that the final minimum

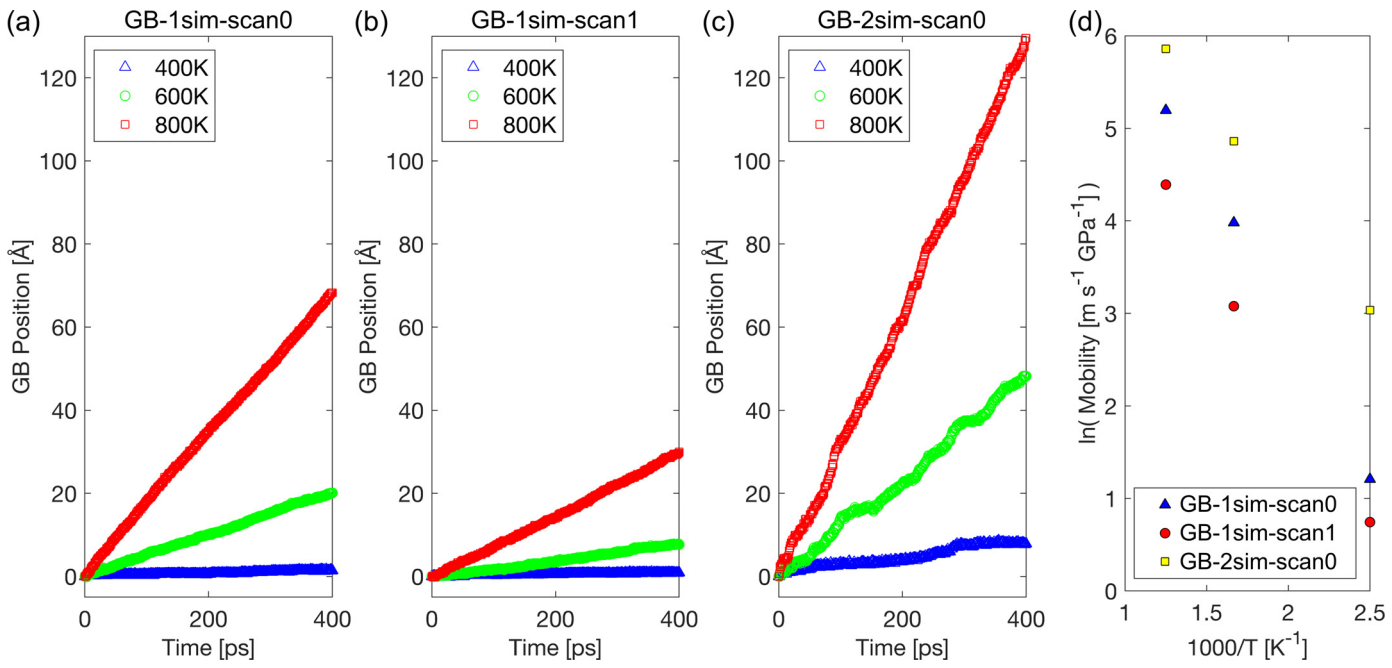

Fig. 3. The average position of the grain boundaries as a function of time at 400 K, 600 K, and 800 K for GB-1sim-scan0 (a), GB-1sim-scan1 (b), and GB-2sim-scan0 (c). (d) The mobilities of the simulated boundaries plotted in an Arrhenius manner.

energy structure represents the overall minimum energy, not necessarily the minimum energy structure for each individual region on the surface of the sphere.

Comparing the two models, the advantages of the spherical grain boundary model are: (1) no need to find a specific CSL misorientation as any misorientation can be easily satisfied, (2) theoretically, any oriented boundary segments can be found on the spherical interface. A disadvantage is that mobility values cannot be resolved with this method, and the migration of any given BP orientation is affected by neighboring BP orientations, and thus by boundary stiffness.

Supplementary Fig. S2 depicts the snapshots of GB atoms of different simulation times during annealing of GB-1exp and GB-2exp at 600 K, indicating that the interior grains shrink in a similar manner in the two cases without significant grain shape changes and no recognizable facet formation. The simulated volume fraction of the recrystallized grains as a function of annealing time for GB-1exp and GB-2exp models is shown in Fig. 4a. Furthermore, we calculated the migration distance of the GB and plotted the result in a stereographic projection in Fig. 4b–d and 4e–g for GB-1exp and GB-2exp, respectively. The plots enable us to estimate roughly which GBs migrate faster at specific temperatures. From these plots, where the circles and triangles respectively mark the target BP orientations at scan0 and scan1, the migration rate of GB-2exp-scan0 is predicted to be slightly higher than GB-1exp-scan0 and GB-1exp-scan1, consistent with the conventional bicrystal model simulation results.

Previous atomistic simulations [17] have demonstrated that when GBs are constrained, as might occur in polycrystalline networks, the relative GB mobilities can be significantly altered. The grain in the present experiment is isolated in the deformed microstructure, so there are no constraints from neighboring grains. The individual segments of the boundary surrounding the grain may of course affect the migration of neighoboring segments and also constraints from the surrounding deformed matrix are likely. It is however impossible to evaluate possible effects of the latter based on the present data.

Based on the present simulations, no correlations between the simulated grain boundary migration and the experimentally observed heterogeneous boundary migration behavior could be identified, either by the bicrystal or the spherical model. Based on the experimental measurements, it was previously established that the local stored energy differences in the deformation microstructures in front of the two boundary segments could not explain the migration behavior [14]. Remaining explanations must thus relate directly to the deformation microstructures, either via a constraint effect as mentioned above or by preferential growth into deformation morphologies with favorably arranged dislocation boundaries as suggested in [11]. Also, recent phase-field simulations of recrystallization in idealized deformation microstructures support that the morphology of the deformation microstructure, and not only the stored energy, is critical in controlling recrystallization [23–25].

In summary, the migration of selected grain boundary segments, mimicking experimental recrystallization observations, are analyzed by atomistic simulations using two models. The simulations reveal that the predicted mobility differences would favor the migration of the boundary segment that is found to be stationary in the experiment over the one that actually migrates. Therefore the mobility difference cannot explain the heterogeneous migration behavior observed in the experiment. The previous experimental work [14] ruled out that differences in stored energy in front of the two boundary segments could be the explanation. Taken together, we must therefore conclude that for the present case $v = M \times f$ is not valid on the *local* scale when considering recrystallization boundary migration. Other factors related to constraints by dislocation boundaries, or preferential growth relationships with favorably arranged dislocation boundaries within the deformation microstructure, must be of critical importance for recrystallization.

Declaration of Competing Interest

The authors declare that they have no known competing financial interests or personal relationships that could have appeared to influence the work reported in this paper.

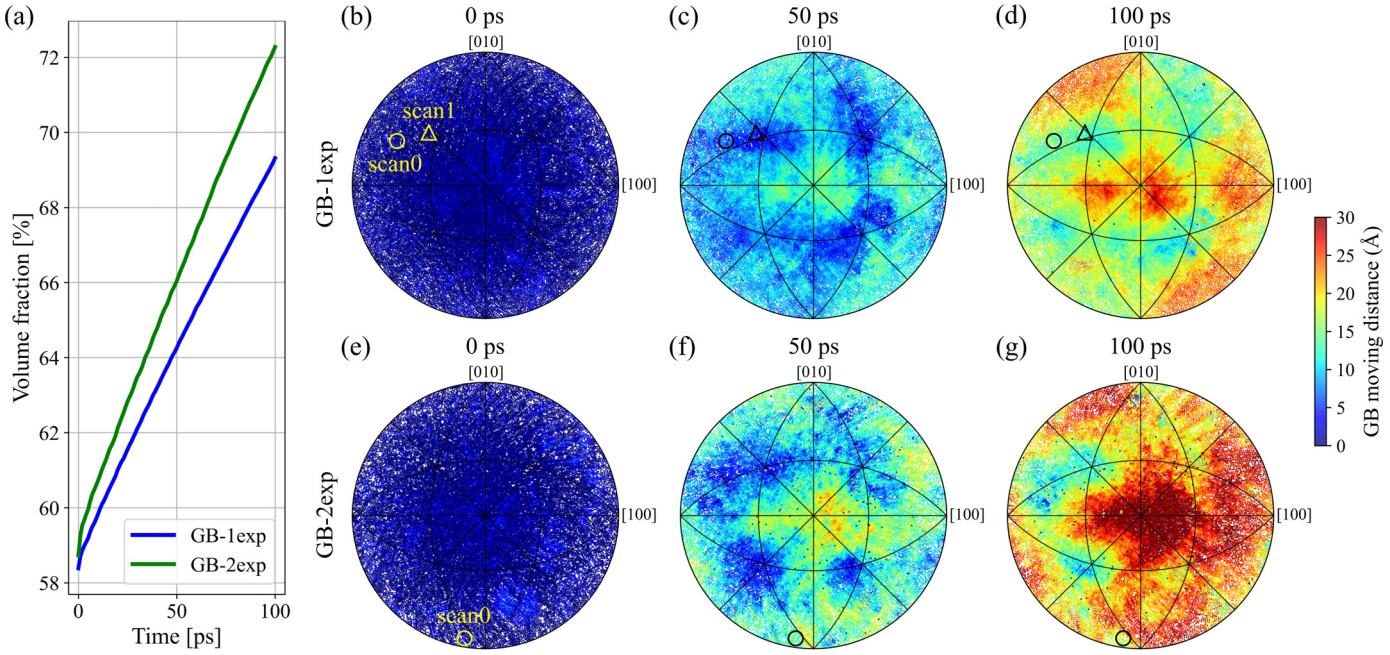

Fig. 4. Spherical bicrystal model simulation results showing the grain boundary migration at 600 K of the two measured misorientations. (a) The simulated volume fraction of recrystallized grains as a function of annealing time for GB-1exp and GB-2exp. The moving distance of the GB atoms: (b-d) GB-1exp. (e-g) GB-2exp at different times. The reference frame for the projection is the crystallographic coordinate system of the recrystallized grains.

Acknowledgments

The authors gratefully acknowledge the financial support from the European Research Council (ERC) under the European Union's Horizon 2020 research and innovation program (M4D-grant agreement No. 788567), within which this work has been performed.

Supplementary materials

Supplementary material associated with this article can be found, in the online version, at doi:10.1016/j.scriptamat.2021.114489.

References

[1] F.J. Humphreys, M. Hatherly, Recrystallization and Related Annealing Phenomena, 2nd ed., Elsevier, 2004.
[2] Z. Jeffries, Part I. Grain Growth in metals: Part II. The effect of Temperature Deformation and Grain Size On the Mechanical Properties of Metals, Harvard Universtiy, 1918.
[3] T.J. Rupert, D.S. Gianola, Y. Gan, K.J. Hemker, Science 326 (2009) 1686–1690.
[4] J.L. Bair, E.R. Homer, Acta Mater. 162 (2019) 10–18.
[5] R. Hadian, B. Grabowski, M.W. Finnis, J. Neugebauer, Phys. Rev. Mater. 2 (2018) 043601.
[6] A. Bhattacharya, Y.F. Shen, C.M. Hefferan, S.F. Li, J. Lind, R.M. Suter, C.E. Krill, G.S. Rohrer, Science 374 (2021) 189–193.
[7] Y. Zhang, A. Godfrey, D. Juul Jensen, Metall. Mater. Trans. A 45 (2014) 2899–2905.
[8] Y. Zhang, J. Budai, J. Tischler, W. Liu, R. Xu, E.R. Homer, A. Godfrey, D. Juul Jensen, Sci. Rep. 7 (2017) 1–8.
[9] S. Schmidt, S. Nielsen, C. Gundlach, L. Margulies, X. Huang, D. Juul Jensen, Science 305 (2004) 229–232.
[10] J. Sun, C. Holzner, H. Bale, M. Tomita, N. Gueninchault, F. Bachmann, E. Lauridsen, T. Inaguma, M. Kimura, ISIJ Int. 60 (2019) 405.
[11] G.H. Fan, Y.B. Zhang, J.H. Driver, D. Juul Jensen, Scripta Mater. 72–73 (2014) 9–12.
[12] G. Gottstein, D.A. Molodov, L.S. Shvindlerman, Interface Sci. 6 (1998) 7–22.
[13] M. Upmanyu, D.J. Srolovitz, L.S. Shvindlerman, G. Gottstein, Acta Mater. 47 (1999) 3901–3914.
[14] C. Hong, Y. Zhang, A. Lindkvist, W. Liu, J. Tischler, R. Xu, D. Juul Jensen, Scripta Mater. 205 (2021) 114187.
[15] E.R. Homer, S. Patala, J.L. Priedeman, Sci. Rep. 5 (2015) 15476.
[16] D.L. Olmsted, S.M. Foiles, E.A. Holm, Acta Mater. 57 (2009) 3694–3703.
[17] E.R. Homer, IOP Conf. Ser. Mater. Sci. Eng. 89 (2015) 012006.
[18] Y. Mishin, D. Farkas, M.J. Mehl, D.A. Papaconstantopoulos, Phys. Rev. B 59 (1999) 3393–3407.
[19] S. Plimpton, J. Comput. Phys. 117 (1995) 1–19.
[20] F. Ulomek, C.J. O'Brien, S.M. Foiles, V. Mohles, Model. Simul. Mater. Sci. Eng. 23 (2015) 025007.
[21] A.A. Schratt, V. Mohles, Comput. Mater. Sci. 182 (2020) 109774.
[22] G. Gottstein, L.S. Shvindlerman, Grain Boundary Migration in metals: Thermodynamics, kinetics, applications, Second Edition, CRC Press, 2009.
[23] N. Moelans, A. Godfrey, Y. Zhang, D. Juul Jensen, Phys. Rev. B 88 (2013) 054103.
[24] V. Yadav, N. Moelans, Y. Zhang, D. Juul Jensen, Scripta Mater. 191 (2021) 116–119.
[25] R. Li, V. Yadav, N. Moelans, Y. Zhang, D. Juul Jensen, IOP Conf. Ser. Mater. Sci. Eng. 1121 (2021) 012013.